



Received: 23/12/2025

Revised: 25/02/2026

Accepted: 19/03/2026

Published online: 30/03/2026

Research Article



Open Access under the CC BY -NC-ND 4.0 license

UDC 532.517:532.135

TURBULENT FLOW OF VISCOELASTIC FLUID BASED ON THE REYNOLDS STRESS MODEL

Zhabbasbayev U.K.¹, Pakhomov M.A.², Ramazanova G.I.¹, Sattinova Z.K.^{3,*}¹ Satbayev University, Almaty, Kazakhstan² Kutateladze Institute of Thermophysics SB RAS, Novosibirsk, Russia³ L.N. Gumilyov Eurasian National University, Astana, Kazakhstan*Corresponding author: sattinova.kz@gmail.com

Abstract. This article presents the results of applying a turbulent stress model to the simulation of high-viscosity viscoelastic fluid flow in a pipe. The model is used to numerically determine averaged velocity and stress fields within the Navier–Stokes equations. The proposed model takes into account the influence of the Sisko fluid rheology on turbulent momentum transfer, providing a physically sound description of the interaction between turbulence and non-Newtonian effects. Calculations for a Newtonian fluid are performed as a baseline for evaluating the effectiveness of the proposed approach. It is shown that for Sisko fluid, the averaged velocity profile in universal coordinates is systematically shifted upward compared to the Newtonian case, indicating weakening of turbulent momentum transfer and a decrease in hydrodynamic drag. It is established that the level of axial velocity fluctuations exceeds the Newtonian value, while radial fluctuations are lower, indicating pronounced anisotropy of turbulent stresses. The viscoelastic properties of the fluid lead to a reduction in turbulent friction due to the suppression of small-scale vortex structures and, as a consequence, to a reduction in the hydraulic resistance of the pipe.

Keywords: highly viscous elastic fluid, Sisko rheological model, turbulent stresses, non-Newtonian effects.

1. Introduction

The phenomenon of drag reduction (DR), present in turbulent viscoelastic flows, has been studied for decades [1-7]. It is well known that the addition of polymer particles to a Newtonian fluid in turbulent flow can achieve a reduction in transfer energy of up to 80% by reducing turbulent friction [1-9]. Another effect is the reduction in heat transfer. Both phenomena provide significant benefits in terms of energy savings for transporting fluids over long distances, and for this reason, researchers are focusing their efforts on its use in engineering systems. Since the discovery of the drag reduction phenomenon, numerous studies have been conducted to understand the origin of drag reduction in turbulent flows, and several theories have been proposed to describe this complex mechanism, but a definitive consensus has not been reached.

The two preferred theories are Lumley's theory [3, 4], known as the viscous idea, and Tabor and De Gennes's theory [8], known as the elastic explanation. Lumley suggests that the phenomenon of drag reduction (DR) is a consequence of an increase in effective viscosity in the region beyond the viscous sublayer and in the buffer layer, caused by polymer stretching in turbulent flow. He also suggests that the onset of drag reduction occurs when the polymer time scale exceeds the flow time scale. Another suggestion by Tabor and De Gennes is that the elastic energy stored in the polymer becomes equivalent to the turbulent kinetic energy

in the buffer layer, suppressing normal energy transfer and thickening the buffer layer where the viscoelastic length scale is greater than the Kolmogorov length scale.

It is known that DR is associated with an increase in the effective elongation viscosity of a dilute polymer solution, which leads to a decrease in vortex dynamic activity, according to Lumley's theory [3, 4]. Later, Lvov et al. [10] quantitatively described the viscous scenario, showing that the additional effective viscosity increases linearly with distance from the wall in the buffer layer. They also proposed direct numerical simulations (DNS) of Newtonian turbulent flows, including artificial viscosity, to validate their theory [11]. This was followed by De Angelis et al. [11], who obtained the same drag reduction properties as the equivalent viscoelastic simulation [12].

However, the DNS results between the two scenarios showed some inconsistencies when considering the high and maximum drag reduction regimes. Recently, Dallas et al. [13] demonstrated that high drag reduction can be achieved without a complete helix-to-stretch transition of polymer molecules, which is contrary to viscous theories. This supports the explanation of Mina et al. [14], in which polymers in the near-wall region extract energy from the flow due to mean-shear-induced unwinding and release some of the stored elastic energy back into the flow by compressing as they move away from the wall.

Although DNS is a powerful tool, it is not applicable to most engineering applications involving turbulent viscoelastic flows. It is significantly more computationally intensive and memory-intensive due to the larger number of primary variables. An alternative approach is to use Reynolds-averaged Navier–Stokes (RANS) models, which are less computationally intensive. Therefore, they have gained increased interest in recent decades. Engineering calculations require turbulence models that accurately describe the average fields and large-scale pulsations of swirling currents. The work of Horvath and Dressel (2012) presents the results of numerical simulation of RANS for a generalized configuration - a single subchannel with lateral periodicity. The authors tested vortex viscosity models and stress transfer models using standard wall functions. The first attempt to incorporate the elastic effect into turbulence models was undertaken by Pinho [15] and Cruz et al. [16].

They developed a $(k-\varepsilon)$ -model of low-Reynolds-number turbulence using the generalized Newtonian fluid (GNF) equation of state. They also developed an anisotropic version that incorporates enhanced Reynolds stress anisotropy (Resende et al., [17]), which is capable of satisfactorily predicting drag reduction. This model is designed to describe the viscoelastic effects responsible for the Toms effect (reduction of hydrodynamic resistance) during turbulent flow in pipelines. Modification of the Launder–Sharma $(k-\varepsilon)$ model by taking into account the rheology of viscoelastic media and using the Cruz – Pinho damping function made it possible to adapt it to calculate dilute non-Newtonian solutions. In this case, the viscoelastic properties are described using a modified generalized Newtonian fluid model (GNF). The authors [16-17] performed a direct numerical simulation corresponding to a statistically converging turbulent fluid flow in the GN channel with a low Reynolds number of friction.

The variable viscosity is taken into account using the Carro model, while the data for the Newtonian case are compared with the results of modeling media exhibiting dilatance and pseudoplasticity properties. The study confirms that variable viscosity affects the internal structure of the flow, where shear thinning dampens wall vortices and banded structures. This inhibits the development of turbulence and leads to the effect of reducing drag.

The main changes in the flow structure include an increase in the longitudinal and suppression of the transverse turbulence intensity, as well as a decrease in the Reynolds shear stresses. In addition, the energy exchange between the components of the stress tensor slows down through the correlation of pressure and velocity, which leads to an increase in the anisotropy of turbulence on small and large scales. In the center of the channel, shear liquefaction enhances the manifestation of specific turbulent structures, which are usually observed at low Reynolds numbers.

In this paper, the RSM model is used to describe the anisotropy of the pulsating velocity components and the reduction of the Reynolds stress.

2. Model mass transfer

2.1 Basic equations

The equations governing the flow are presented in vector symbols, although they are solved for axisymmetric flow in cylindrical coordinates. The system of stationary axisymmetric RANS equations of continuity, momentum in the axial and radial directions of a turbulent incompressible generalized Newtonian fluid has the form [18-20]:

$$\nabla \cdot (\rho \mathbf{U}) = 0 \quad (1)$$

$$\nabla \cdot (\rho \mathbf{U} \mathbf{U}) = -\nabla P + \nabla \cdot (2\mu_{eff} \mathbf{S}) + \nabla \cdot (-\rho \langle \mathbf{u}' \mathbf{u}' \rangle) + \nabla \cdot \langle 2\mu'_{eff} \mathbf{S}' \rangle \quad (2)$$

Here ρ , μ_{eff} expressions of density, effective molecular viscosity of a fluid, respectively. $\mathbf{U} \equiv (u_x, u_r)$ expresses the velocity vector with components ($u_x = U$, $u_r = V$) fluids in axial (x) and radial (r) coordinates, respectively; P express pressure; $-\rho \langle \mathbf{u}' \mathbf{u}' \rangle$ express the Reynolds friction stresses. Expression $\nabla \cdot \langle 2\mu'_{eff} \mathbf{S}' \rangle$ in equation (2) is found according to the representation [18,20]. Turbulent Reynolds stresses $-\rho \langle \mathbf{u}' \mathbf{u}' \rangle = -\rho \langle u_i u_j \rangle$ were found according to the Boussinesq hypothesis [21]. Turbulent viscosity μ_T is determined by using the RSM turbulent stress model [22, 23].

2.2 The RSM Turbulence model

The elliptical relaxation model of turbulent stresses RSM [22] takes into account the anisotropy of complex turbulent flows and is computationally more complex than the known (k- ε) - turbulence model. The RSM model shows better results than (k- ε) isotropic turbulence model. The Reynolds stress components are derived from a system of partial differential equations, and the system of governing equations of the second moment closure model [23] is given below:

$$\begin{aligned} \frac{\partial}{\partial x_j} (\rho U_j \langle u'_i u'_j \rangle) &= \rho (P_{ij} + \phi_{ij} - \varepsilon_{ij}) + \frac{\partial}{\partial x_l} \left[\rho \nu_{eff} \delta_{lm} + \rho \frac{C_\mu T_T}{\sigma_k} \langle u'_l u'_m \rangle \right] \frac{\partial}{\partial x_m} \langle u'_i u'_j \rangle \\ \frac{\partial}{\partial x_j} (\rho U_j \varepsilon) &= \frac{1}{T_T} (C_{\varepsilon 1} \tilde{P} - C_{\varepsilon 2} \varepsilon) + \frac{\partial}{\partial x_l} \left[\rho \nu_{eff} \delta_{lm} + \rho \frac{C_\mu T_T}{\sigma_\varepsilon} \langle u'_l u'_m \rangle \right] \frac{\partial \varepsilon}{\partial x_m} \\ \chi - L_T^2 \nabla^2 \chi &= 1. \end{aligned} \quad (3)$$

Here, P_{ij} and $\tilde{P} = 0.5 \tilde{P}_{kk}$ are intensity of the energy transfer from the average velocity to the fluctuating motion (stress production terms), ϕ_{ij} is redistribution term [23], $L_T = \max \left(\frac{k^{3/2}}{\varepsilon}, C_\eta \frac{\nu^{3/4}}{\varepsilon^{1/4}} \right)$ and

$T_T = \max \left(\frac{k}{\varepsilon}, C_T \sqrt{\frac{\nu}{\varepsilon}} \right)$ are turbulent time and length macroscales, where $2k = \langle u'_i u'_i \rangle$ is the turbulent kinetic

energy, ε_{ij} is viscous dissipation rate tensor of turbulent stresses, $\varepsilon = 0.5 \varepsilon_{kk}$, and χ is a blending coefficient, and it changes from zero at the wall to unity far from the wall [23]. The constants and model functions of the system of equations (3) are given in [23]. The effect of the rate of dissipation of the turbulent kinetic energy is ignored in this model. This term can dominate over the mean flow viscous dissipation in a developing turbulent flow. The NF at the inlet is fully developed and this effect can be neglected.

2.3 Boundary conditions

The flow diagram is shown in Fig. 1.

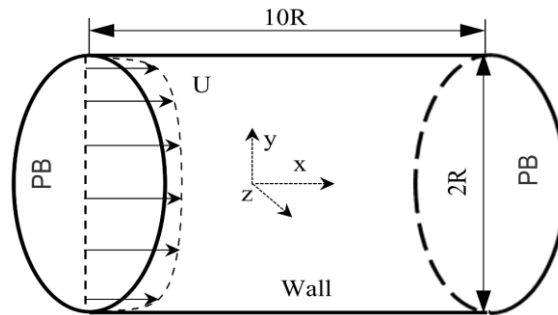


Fig.1. Computational domain for flow in a pipe.

On the wall surface, the conditions of no slip for the velocity are specified [23]:

$$r = R; U = V = \overline{u_i u_j} = 0; \varepsilon = 2\nu_w \frac{k}{y^2}; \chi = 0 \tag{4}$$

Symmetry conditions for all variables are specified on the pipe axis.

$$r = 0; \frac{\partial U}{\partial r} = V = 0; \frac{\partial \overline{u_i u_j}}{\partial r} = \frac{\partial \varepsilon}{\partial r} = \frac{\partial \chi}{\partial r} = 0 \tag{5}$$

At the inlet section ($x = 0$), distributions of all variables across the pipe cross-section are specified, corresponding to developed turbulent flow in the pipe. At the outlet edge ($x = L$), soft boundary conditions are specified for all variables. Numerical modeling of the system of equations (1)-(3) under boundary conditions (4), (5) is presented in [21, 24].

3. Discussion of calculated data

An isothermal turbulent flow of a 0.2% XG xanthan gum solution in a pipe with an internal diameter (ID) $D = 2R = 0.15$ m and a length $L = 3$ m is considered. The average mass velocity of the liquid flow at the inlet of the pipe was $U_{m1} = 4,0$ m/s. Fluid flow density at the inlet section $\rho_1 = 998$ kg/m³.

The Reynolds number of the flow, determined from the flow parameters at the inlet, $Re = U_{m1}D_1/\nu_{W1} = 8300$. The axial velocity profile at the pipe inlet corresponds to a developed flow, and other characteristics of a turbulent flow correspond to this. The Sisco model for a viscoelastic fluid (shear-thinning fluid) [25] viscosity is determined by the formula for 0.2% XG:

$$\mu_{eff} = \mu_{ref} (\lambda_S \dot{\gamma})^{n-1} + \mu_0 \tag{6}$$

In equation (6) μ_{ref} and λ_S – viscosity and time constant in the Sisco model, μ_0 – shear viscosity in the Sisco model, $\dot{\gamma} = \sqrt{2S_{ij}S_{ij}} = S$ – shear rate tensor (Table 1), $S_{ij} = 0.5 \left(\frac{\partial U_i}{\partial x_j} + \frac{\partial U_j}{\partial x_i} \right)$ – strain rate tensor.

Table 1. Properties of viscoelastic fluid according to [24].

$\mu_{ref}, \text{Pa}\cdot\text{s}$	λ_S, s	$\mu_0, \text{Pa}\cdot\text{s}$	n
58.1	1900	0.0016	0.34

Here $u_* = \sqrt{\tau_w / \rho}$ – friction speed, $y^+ = yu_* / \nu_w$, $y = R - r$ – distance from the pipe wall along the normal, τ_w – shear stress, ν_w and ρ – kinematic viscosity determined from the parameters on the wall and the density of the medium.

Figure 2, a shows the averaged axial velocity profiles in universal coordinates for a Newtonian fluid (NF) and a non-Newtonian, viscoelastic fluid (NNF). The standard logarithmic law-of-the-wall profile of turbulent flow in a pipe at high Reynolds numbers (Re) for the Newtonian fluid is also plotted. At Reynolds number $Re = 8300$, the averaged axial velocity profile for the Newtonian fluid in the laminar sublayer has the same law-of-the-wall distribution.

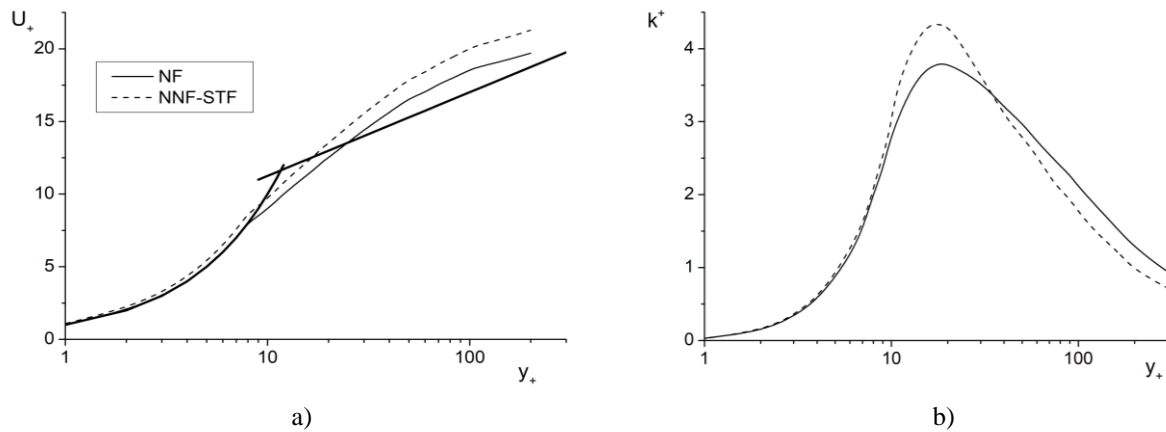


Fig.2. Averaged axial velocity profiles $U^+ = U / u_*$ (a), kinetic energy of turbulence $k^+ = k / u_*^2$ (b) in universal coordinates.

In the core of the current $y^+ = yu_* / \nu_w > 50$ the average axial velocity (NF) profile lies above the linear logarithmic profile, which corresponds to the laws of turbulent flow in a pipe at low Re numbers. The averaged axial velocity profile for a non-Newtonian viscoelastic fluid (NNF) lies even higher than the profile of a Newtonian fluid (NF) in the turbulent core of the flow (see Fig. 2, a). This is explained by the fact that vortices in the viscoelastic fluid accelerate the flow, causing the profile to stretch in the core of the flow.

The distribution of turbulent kinetic energy of a viscoelastic fluid shows an increase in the value in the buffer zone of the flow compared to the distribution of a Newtonian fluid (see Fig. 2,b). As can be seen from Fig. 2,b, the maximum value of turbulent kinetic energy is reached at a value of $y^+ = yu_* / \nu_w = 20$. Turbulent kinetic energy in both Newtonian and viscoelastic fluids reaches its maximum value in the buffer zone (see Fig. 2, b).

Figure 3 shows the profiles axial $u'^+ = u' / u_*$ (a) and radial $v'^+ = v' / u_*$ (b) fluctuations and Reynolds stresses $\langle uv \rangle^+ = \langle u'v' \rangle / u_*^2$ (c) in universal coordinates. The turbulent stress model (RSM) describes the anisotropic property of turbulent flow in a pipe. As can be seen from Figure 3, the profiles axial $u'^+ = u' / u_*$ (a) and radial $v'^+ = v' / u_*$ (b) fluctuations have different distribution patterns. If the axial fluctuation profile $u'^+ = u' / u_*$ reaches its maximum value at $y^+ = yu_* / \nu_w < 20$, then, as radial fluctuation profile $v'^+ = v' / u_*$ reaches its maximum value at $y^+ = yu_* / \nu_w < 80$, i.e. at a significantly greater distance from the pipe wall (see Fig. 3). It should be noted that the maximum value of the axial fluctuation profile $u'^+ = u' / u_*$ viscoelastic fluid is greater than Newtonian fluid (see Fig. 3, a). Then, as the maximum value of the radial fluctuation profile $v'^+ = v' / u_*$ less than Newtonian fluid (see Fig. 3, b).

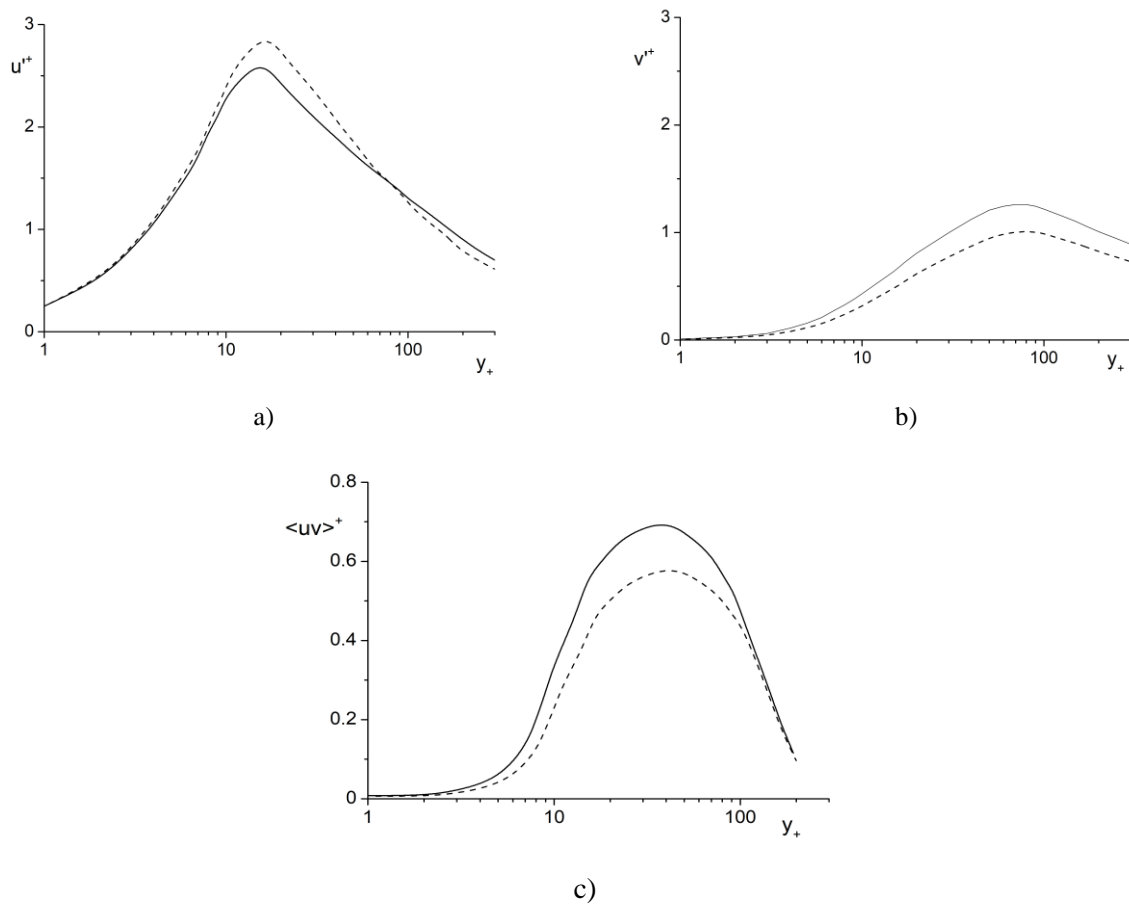


Fig.3. Axial $u'^+ = u' / u_*$ (a) and radial $v'^+ = v' / u_*$ (b) profiles fluctuations and Reynolds stress $\langle uv \rangle'^+ = \langle u'v' \rangle / u_*^2$ (c) in universal coordinates.

Varied distribution of profiles axial $u'^+ = u' / u_*$ and radial $v'^+ = v' / u_*$ fluctuation leads to the form of Reynolds stress $\langle uv \rangle'^+ = \langle u'v' \rangle / u_*^2$ in universal coordinates (see Fig. 3,c). Reynolds stress distribution $\langle uv \rangle'^+ = \langle u'v' \rangle / u_*^2$ viscoelastic fluid (dashed line) passes below the Reynolds stress distribution $\langle uv \rangle'^+ = \langle u'v' \rangle / u_*^2$ Newtonian fluid (see Fig. 3, c). Turbulent flow friction determined by the Reynolds stress $\langle uv \rangle'^+ = \langle u'v' \rangle / u_*^2$, decreases in viscoelastic fluid compared to a Newtonian one.

Thus, the viscoelastic property of the fluid causes a decrease in turbulent friction and hydraulic resistance of the flow.

4. Conclusion

The paper demonstrates that the use of a turbulent stress model allows one to accurately describe the turbulent flow characteristics of a non-Newtonian viscoelastic fluid in a pipe without directly resolving all turbulence scales. A comparison with the Newtonian case allowed us to quantify the contribution of non-Newtonian effects due to the rheology of Sisko fluid to the formation of velocity and turbulent stress profiles. It was found that the averaged velocity profile in universal wall-layer coordinates for Sisko fluid lies above the corresponding profile for a Newtonian fluid, which is due to a decrease in effective viscosity with increasing shear rate. It was shown that the turbulent kinetic energy profile for Sisko fluid is more elongated compared to the Newtonian case, indicating weakening of local turbulent energy dissipation. Significant differences between the axial and radial fluctuation velocity profiles indicate pronounced anisotropy of turbulent stresses and confirm the model's ability to adequately reproduce this flow property. The obtained

effect of reducing hydrodynamic resistance confirms the correctness of taking into account the viscoelastic properties of the fluid in the proposed model of turbulent stresses.

Conflict of interest statement

The authors declare that they have no conflict of interest in relation to this research, whether financial, personal, authorship or otherwise, that could affect the research and its results presented in this paper.

CRedit author statement

Zhapbasbayev U.K.: Conceptualization, Funding acquisition, Supervision; **Pakhomov M.A.:** Investigation, Methodology, Validation; **Ramazanova G.I.:** Formal analysis, Writing – original draft; **Sattinova Z.K.:** Data curation, Writing Reviewing and Editing. The final manuscript was read and approved by all authors.

Funding

This work was supported by the Science Committee of the Ministry of Science and Higher Education of the Republic of Kazakhstan (Grant No's. AP23486543 for 2024-2026)

References

- 1 Toms B.A. (1948) Some observations on the flow of linear polymer solutions through straight tubes at large Reynolds numbers. *Proc. Int. Cong. Rheol.*, 2, 135–141. <https://ci.nii.ac.jp/naid/10004666161>
- 2 Bayode E.Owolabi, David J.C.Dennis & Robert J.Poole (2017) Turbulent drag reduction by polymer additives in parallel shear flows. *J. of fluid Mechanics*, 827. <https://doi.org/10.1017/jfm.2017.544>
- 3 Sellin R.H. J., Hoyt J.W.& Scrivener O. (1982) The effect of Drag-Reducing Additives on fluid flows and their industrial applications. *J. of Hydraulic Research*, 20(1), 29–68. <https://doi.org/10.1080/00221688209499499>
- 4 Berman N.S. (1989) Polymer contributions to transport equations. In Drag reduction in fluid flows. *Techniques for Friction Control*, 21. https://link.springer.com/chapter/10.1007/978-3-7091-2574-8_10
- 5 Keizo Watanabe, Satoshi Ogata. (2023) Drag Reduction by Complex Mixtures in Turbulent Pipe Flows. *Flow, Turbulence and Combustion*, 113, 41-49. <https://doi.org/10.1007/s10494-023-00448-9>
- 6 Zhapbasbayev U.K., Bossinov D.Zh., Pahomov M.A., Sattinova Z. (2025) Modeling of Turbulent Non-Isothermal Flow in a Heating Network Pipe. *Bulletin of The Karaganda University. Physics Series*, 30, 2(118), 67-74. <https://doi.org/10.31489/2025ph2/67-74>
- 7 Thais L., Gatski T.B. & Mompean G. (2012) Some dynamical features of the turbulent flow of a viscoelastic fluid for reduced drag. *J. Turbul.* 13, N19. <https://doi.org/10.1080/14685248.2012.685522>
- 8 Tabor M. & De Gennes P.G. (1986) A cascade theory of drag reduction. *EPL. Europhys. Lett.*, 2 (7), 519. <https://doi.org/10.1209/0295-5075/2/7/005>
- 9 Ptasincki P.K., Boersma B.J., Nieuwstadt F.T.M., Hulsen M.A., Van der Brule B.H.A.A., & Hunt J.C.R. (2003) Turbulent channel flow near maximum drag reduction: simulations, experiments and mechanisms. *J. Fluid Mech.*, 490, 251-291. <https://doi.org/10.1017/S0022112003005305>
- 10 L'vov V.S., Pomyalov A., Procaccia I. & Tiberkevich V. (2004) Drag reduction by polymers in wall bounded turbulence. *Phys. Rev. Lett.*, 92, 244503. <https://doi.org/10.1103/PhysRevLett.92.244503>
- 11 De Angelis E.; Casciola C.M.; L'vov V.S.; Pomyalov A.; Procaccia I.; & Tiberkevich V. (2004) Drag reduction by a linear viscosity profile. *Phys. Rev. E.*, 70, 055301(R). <https://doi.org/10.1103/PhysRevE.70.055301>
- 12 Sureshkumar R.; Beris A.N.; & Handler R.A. (1997) Direct numerical simulation of the turbulent channel flow of a polymer solution. *Phys. Fluids*, 9, 743–755. <https://doi.org/10.1063/1.869229>
- 13 Dallas V., Vassilicos J.C.; & Hewitt G.F. (2010) Strong polymer-turbulence interactions in viscoelastic turbulent channel flow. *Phys. Rev. E*, 82, 066303. <https://doi.org/10.1103/PhysRevE.82.066303>
- 14 Min T., Yoo J.Y., Choi H., Joseph D.D. (2003) Drag reduction by polymer additives in a turbulent channel flow. *J. Fluid Mech.*, 486, 213–238. <https://doi.org/10.1017/S0022112003004610>
- 15 Pinho F. A. (2003) GNF framework for turbulent flow models of drag reducing fluids and proposal for a $k - \epsilon$ type closure. *J. Non-Newton. Fluid Mech.*, 114, 149–184. [https://doi.org/10.1016/S0377-0257\(03\)00120-4](https://doi.org/10.1016/S0377-0257(03)00120-4)
- 16 Cruz D.; Pinho F.; & Resende P. (2004) Modelling the new stress for improved drag reduction predictions of viscoelastic pipe flow. *J. Non-Newton. Fluid Mech.*, 121, 127–141. <https://doi.org/10.1016/j.jnnfm.2004.05.004>
- 17 Resende P.; Escudier M.; Presti F.; Pinho F.; & Cruz D. (2006) Numerical predictions and measurements of Reynolds normal stresses in turbulent pipe flow of polymers. *Int. J. Heat Fluid Flow*, 27, 204 – 219. <https://doi.org/10.1016/j.ijheatfluidflow.2005.08.002>
- 18 Gavrilov A.A., & Rudyak, V.Y. (2016). Reynolds-averaged modeling of turbulent flows of power-law fluids, *J. Non-Newton. Fluid Mech.*, 227, 45–55. <https://doi.org/10.1016/j.jnnfm.2015.11.006>

- 19 Sakipova S.E., Shaimerdenova K.M., Nussupbekov, Ospanova D.A., Kutum B.B. (2023) Modeling the dynamics of heat and mass transfer processes in a tubular heat exchanger under pulsed influences. *Eurasian Physical Technical Journal*, 20, 1(43), 51-55. <https://doi.org/10.31489/2023No1/51-55>
- 20 Lovato S., Keetels G.H., Toxopeus S.L. & Settels J.W. (2022) An eddy-viscosity model for turbulent flows of Herschel–Bulkley fluids. *J. Non-Newtonian Fluid Mech.*, 301 104729. <https://doi.org/10.1016/j.jnnfm.2021.104729>
- 21 Pakhomov M.A., & Zhapbasbayev U.K. (2024) Comparative predictions of turbulent non-isothermal flow of a viscoplastic fluid with a yield stress. *Heliyon*, 10e24062. <https://doi.org/10.1016/j.heliyon.2024.e24062>
- 22 Manceau R. & Hanjalić K. (2002) Elliptic blending model: a new near-wall Reynolds-stress turbulence closure. *Phys. Fluids*, 14(2) 744–754. <https://doi.org/10.1063/1.1432693>
- 23 Fadai-Ghotbi A., Manceau R. & Boree J. (2006) Revisiting URANS computations of the backward-facing step flow using second moment closures. Influence of the numerics. *Flow, Turbulence and Combust.*, 81(3) 395–410. https://doi.org/10.1007/978-3-540-92779-2_79
- 24 Pakhomov M.A. & Zhapbasbayev U.K. (2024) RANS Predictions of Turbulent Non-Isothermal Viscoplastic Fluid in Pipe with Sudden Expansion. *Journal of Non-Newtonian Fluid Mechanics*, 334, 105329, <https://doi.org/10.1016/j.jnnfm.2024.105329>
- 25 Pereira A.S., & Pinho F.T. (2000) Turbulent characteristics of shear-thinning fluids in recirculating flows. *Exp. Fluids*, 28, 266–278. <https://doi.org/10.1007/s003480050387>

AUTHORS' INFORMATION

Zhapbasbayev Uzak Kairbekovich – Doctor of Technical Sciences, Professor, Head of the Research and Production Laboratory "Modeling in Energy", Satbayev University, Almaty, Kazakhstan; Scopus ID: 6508298888; <https://orcid.org/0000-0001-5973-5149>, uzak.zh@mail.ru,

Pakhomov Maksim Aleksandrovich – Doctor of Physical and Mathematical Sciences, Major Research Worker, Kutateladze Institute of Thermophysics SB RAS, Novosibirsk, Russian Federation. Scopus ID: 6602734341; <https://orcid.org/0000-0002-8127-3638>, Pakhomov@itp.nsc.ru

Ramazanov Gaukhar Izbasarovna – Candidate of Physical and Mathematical Sciences, Deputy Head of "Modeling in Energy", Satbayev University, Almaty, Kazakhstan; Scopus ID: 6506885857; ORCID: <https://orcid.org/0000-0002-8689-9293>, gaukhar.ri@gmail.com

Sattinova Zamira Kanaevna - Candidate of physical and mathematical sciences, Acting Professor, L.N. Gumilyov Eurasian National University, Astana, Kazakhstan; Scopus ID: 54400166600; <https://orcid.org/0000-0002-2990-6581>; sattinova.kz@gmail.com